Deep Data-Driven Neural Network for Malaria Vaccination

Preprint · January 2025

DOI: 10.21203/rs.3.rs-5789145/v1

2 authors, including:

Stephen E. Moore
University of Cape Coast
63 PUBLICATIONS **887** CITATIONS

SEE PROFILE

Deep Data-Driven Neural Network for Malaria Vaccination

Esi Abaka-Quansah
African Institute of Mathematical Science, Mbour, Senegal
Stephen E. Moore
stephen.moore@ucc.edu.gh

Department of Mathematics, University of Cape Coast

Research Article

Keywords: Malaria Vaccination, deep learning, ResNet, RNN, k-fold cross validation

Posted Date: January 10th, 2025

DOI: https://doi.org/10.21203/rs.3.rs-5789145/v1

Additional Declarations: The authors declare no competing interests.

Deep Data-Driven Neural Network for Malaria Vaccination

Esi Abaka-Quansah[1] and Stephen E. Moore*[2]

[1]African Institute of Mathematical Science, Senegal
[2]Department of Mathematics, University of Cape Coast, Cape Coast, Ghana

Abstract

Malaria still remains a significant global health challenge that requires innovative strategies for its control and eventual eradication. In this article, we present a malaria vaccination model to assess and predict the effects of vaccination interventions. The model parameters are learned via feedforward Neural Network. We employed Residual Neural Network and Recurrent Neural Networks(GRU, LSTM, and BiLSTM) to predict and forecast daily and sequential malaria cases using generated data from the Ghana vaccination population.

Keywords: Malaria Vaccination, deep learning, ResNet, RNN, k-fold cross validation

1 Introduction

Malaria is a major worldwide health challenge, especially in Sub-Saharan Africa, where it is most severe among vulnerable groups such as newborns and pregnant women. Despite decades of joint efforts to control the disease, progress has been hindered by pesticide resistance, drug resistance, and limited access to treatment options. Currently, malaria kills approximately 2-3 million people annually. Although the adoption of malaria prevention methods such as chemotherapy and insecticide-sprayed bed nets could significantly lower mortality, an effective malaria vaccine is still needed [11]. Introducing malaria vaccination is a great chance to strengthen existing control strategies and enhance progress toward malaria elimination. The introduction of malaria vaccine has been a significant advance toward elimination. Promising malaria vaccines have been developed and implemented in endemic regions thanks to recent advances in science and technology, and in some Sub-Saharan African countries. Now, vaccines have the potential to reduce malaria-related morbidity and mortality, especially in high-risk populations. Nevertheless, the effectiveness of vaccination programs depends on several factors including vaccine efficacy, coverage, and the dynamics of malaria transmission [21].

According to Adrian [5], the development of malaria vaccines has led to the examination of many innovative vaccination technologies including vector-based prime-boost treatments, innovative supplements, and the concept of community immunization to limit malaria transmission. A protein in the supplement vaccine, which works through antibodies against microorganisms and viral vector vaccines that target the intracellular liver stage parasite with cellular immunity, revealed some efficacy in individuals during phase III trials for antisporozoite vaccination [5].

*Corresponding author: stephen.moore@ucc.edu.gh

The World Health Organization [22] announced that twelve African countries will receive 18 million doses of the RTS,S/AS01 malaria vaccine between 2023 and 2025 due to high demand. This initiative marks a major step forward in combating malaria, a leading cause of death in Africa. Since 2019, Ghana, Kenya, and Malawi have been using the vaccine. Nine additional countries - Benin, Burkina Faso, Burundi, Cameroon, the Democratic Republic of the Congo, Liberia, Niger, Sierra Leone, and Uganda - will now integrate the vaccine into their immunization programs, expanding its reach across the continent.

To maximize the impact of malaria vaccination efforts, it is essential to develop advanced models that can accurately predict the outcomes of vaccination campaigns. These models need to take into consideration the complex interactions between various factors including vaccination features, vector ecology, and population demography. They also need to be able to predict how vaccinations will affect the dynamics of malaria transmission in the long run and evaluate the likelihood of reaching the disease's eradication targets. Deep data-driven models present a promising way to overcome these shortcomings by combining various data sources and utilizing advanced computational techniques to simulate and predict the results of vaccination interventions [7].

Data-driven models consist of a family of mathematical or computational models that derive their parameters, structure, and functionality directly from data. These models do not mainly rely on specific theoretical presumptions or subject expertise; instead, they are developed using observed data trends. These models evolved from previous statistical models that were constrained by rigid assumptions about probability distributions. They have become more prevalent in many domains, especially in the eras of big data, AI, and machine learning, where they provide insightful analysis and predictions based on the available data [2]. Some examples include fuzzy reasoning, which involves addressing uncertainty using fuzzy and rough sets, approximating functions with neural networks, global optimization and evolutionary computing, statistical learning theory, and Bayesian techniques [18]. These models have also gained importance in several industries, including military, financial services, healthcare, economics, and customer relations management [15]. Significant contributions to data-driven modeling includes the development of Physics-Informed Neural Networks (PINNs) by George E. Karniadakis and his fellow collaborators [14], the Sparse Identification of Nonlinear Dynamics (SINDy) introduced by Brunton et al. (2016) [4], the Disease-Informed Neural Network built on the successful Physics-Informed Neural Networks [17] and Hybrid Models combining data-driven and equation-based approaches [25]. PINNs ensures that the resulting model not only fits the data but also respects the underlying physical principles enabling applications in fluid dynamics, heat transfer, and structural mechanics.[14, 13]. SINDy uses sparse regression techniques to identify governing equations from data ranging from fluid dynamics to epidemiology, providing interpretable models that balance accuracy and simplicity [4]. DINNs are employed to predict the spread of infectious diseases[17]. Despite their successes, data-driven approaches face challenges, such as the need for large, high-quality datasets and the possibility for overfitting [19]. These problems are intended to be addressed by recent developments in uncertainty quantification and transfer learning [24].

In epidemiology, data-driven models are formulated to study and analyze health-related issues or occurrences in populations and their distribution. These models play a major role in understanding the spread of disease, forecasting outbreaks, and assessing measures for prevention within a given time. They are also essential for monitoring and assessing epidemics, forecasting their evolution, and supporting timely decision-making to manage healthcare and socioeconomic impacts [3]. Some commonly

applied data-driven models used in epidemiology includes:

- **SIR Models:** This is one of the fundamental compartmental models for understanding the transmission of infectious diseases. The population is divided into three compartments: Susceptible (S), Infected (I), and Recovered (R). Differential equations are frequently defined using real-world data to determine the transitions between these compartments.
- **SEIR Models:** Like SIR models, SEIR models include an extra compartment (E) for those exposed but not yet contagious [9]. This is useful for diseases with a latent period.
- **Agent-Based Models (ABMs)**: These models replicate the behaviours and interactions of individual agents in a population. Every agent could have different traits and ways of acting [8]. ABMs are useful for researching diverse populations, complex disease dynamics and the results of an individual's level of treatment.
- **Machine Learning Models:** Machine learning methods are used frequently to address epidemiological issues due to the emergence of big data in healthcare. These models could analyse large datasets to find trends, forecast disease outbreaks and guide choices. Examples include the use of statistical methods to identify high-risk populations or neural networks for disease prediction such as Residual Neural Networks (ResNet), Recurrent Neural Networks (RNN) and others.

The rest of the paper is organized as follows; In Section 2, Section 3, Section 4, Section 5

2 Mathematical Model Formulation

The susceptible population is denoted as S, the infected population as I, and the recovered population after malaria infection as R. The first dose (V_1) of malaria vaccine is administered at 5-6 months of age, the second dose V_2 at 7 months of age, the third dose (V_3) at 9 months of age, and the last dose (V_2) within 15-18 months of age at a given rate a given rate ρ_i, $i = 1, 2, 3, 4$, increasing the vaccine's efficacy η_i, $i = 1, 2, 3, 4$. In this epidemical model, new births enter the susceptible population at a constant Λ.

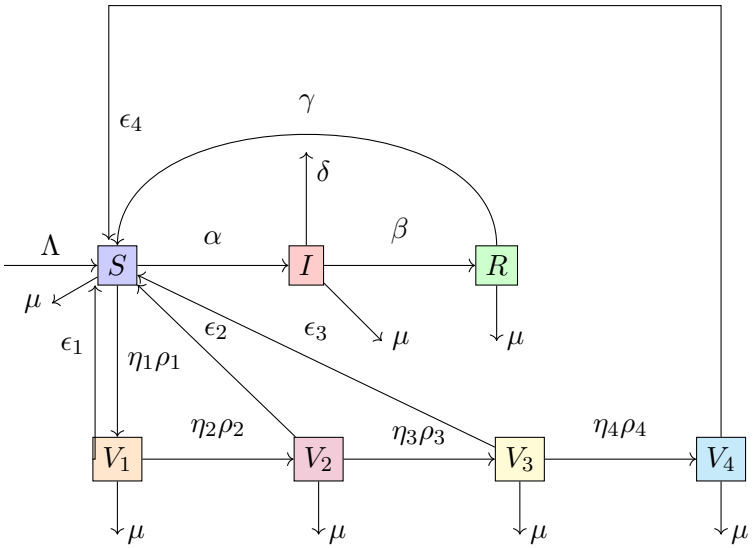

Figure 1 Flow chart indicating the dynamics of Malaria Vaccination model

Based on Figure 1, the dynamics of the vaccination model can be mathematically represented by the following system of ordinary differential equations:

Parameter	Description
Λ	Birth rate
α	Rate of infection
β	Rate of recovery
γ	Rate of losing immunity from recovery population
δ	Disease-induced death rate
μ	Natural mortality rate of infants
η_i	efficacy of each ith vaccine
ρ_i	rate of vaccinated infants at the ith vaccine intake
ϵ_i	Rate of losing immunity after ith vaccine intake

Table 1 Description of Parameters Used in the Equations

$$\begin{cases} \frac{dS}{dt} &= \Lambda - \alpha SI + \gamma R - \mu S - \eta_1\rho_1 S + \epsilon_i \sum_{i=1}^{4} V_i \\ \frac{dI}{dt} &= \alpha SI - (\beta + \delta + \mu)I \\ \frac{dR}{dt} &= \beta I - (\gamma + \mu)R \\ \frac{dV_1}{dt} &= \eta_1\rho_1 S - (\epsilon_1 + \eta_2\rho_2 + \mu)V_1 \\ \frac{dV_2}{dt} &= \eta_2\rho_2 V_1 - V_2\epsilon_2 - \eta_3\rho_3 V_2 - \mu V_2 \\ \frac{dV_3}{dt} &= \eta_3\rho_3 V_2 - V_3\epsilon_3 - \eta_4\rho_4 V_3 - \mu V_3 \\ \frac{dV_4}{dt} &= \eta_4\rho_4 V_3 - V_4\epsilon_4 - \mu V_4 \end{cases} \tag{1}$$

with initial conditions;

$$S(0) > 0, I(0) \geq 0, R(0) \geq 0, V_1(0) \geq 0, V_2(0) \geq 0, V_3(0) \geq 0, V_4(0) \geq 0, t > 0$$

3 Mathematical Analysis

This study examines the possibility of eliminating malaria by incorporating vaccines to reduce the disease's impact and regulate its transmission. Furthermore, the dynamics of the disease are based on its spread, how it affects the total infant population, and how well vaccination programs work to lower the malaria burden. Accordingly, the study's overall framework is as follows. The next sections entail the qualitative analysis of the dynamic system of the mathematical equations. We examine its boundedness, positivity of the solution, equilibria state, stability analysis, the reproductive number R_0, and sensitivity analysis of each parameter in the model.

3.1 Boundedness of the model

The boundedness of the model defines the region in which the solution of the system of equations is non-negative and biologically reasonable. This is essential for interpreting and validating the model's predictions, offering insights into the system's behaviour and stability over time.

Lemma 1. *All solutions of model (1) are bounded in the feasible region* $\mathbf{R}_+^7$.

Proof. See [1, chapter 3]. □

3.2 Positivity of solutions

The positivity of the solutions is also referred to as the non-negativity of solutions of the malaria model equations. Determining the positivity of solutions guarantees a meaningful biological interpretation of the model's predictions as the negativity of solutions represents a lack of physical relevance

Lemma 2. *All solutions of model (1) are positive.*

Proof. See [1, chapter 3]. □

3.3 Stability Analysis

In this section, we determine the model's equilibrium points at both the disease-free and endemic states, compute the local and global stability at these equilibrium points and calculate the reproductive number.

3.3.1 Disease-Free Equilibrium (DFE) Point

This project focuses on vaccination towards malaria elimination hence we consider an equilibrium point within the population where no infections exist. We denote equilibrium point as $(S^*, I^*, R^*, V_1^*, V_2^*, V_3^*, V_4^*)$. The model's equilibrium state is derived by equating the conditions

$$\frac{dS}{dt} = \frac{dI}{dt} = \frac{dR}{dt} = \frac{dV_1}{dt} = \frac{dV_2}{dt} = \frac{dV_3}{dt} = \frac{dV_4}{dt} = 0$$

The system of equations is now written as;

$$\begin{cases} \frac{dS}{dt} &= \Lambda - \alpha S^* I^* + \gamma R^* - \mu S^* - \eta_1\rho_1 S^* + \sum_{i=1}^{4} V_i^* \epsilon_i = 0 \\ \frac{dI}{dt} &= \alpha S^* I^* - (\beta + \delta + \mu) I^* = 0 \\ \frac{dR}{dt} &= \beta I^* - (\gamma + \mu) R^* = 0 \\ \frac{dV_1}{dt} &= \eta_1\rho_1 S^* - (\epsilon_1 + \eta_2\rho_2 + \mu) V_1^* = 0 \\ \frac{dV_2}{dt} &= \eta_2\rho_2 V_1^* - (\epsilon_2 + \eta_3\rho_3 + \mu) V_2^* = 0 \\ \frac{dV_3}{dt} &= \eta_3\rho_3 V_2^* - (\epsilon_3 + \eta_4\rho_4 + \mu) V_3^* = 0 \\ \frac{dV_4}{dt} &= \eta_4\rho_4 V_3^* - (\epsilon_4 + \mu) V_4^* = 0. \end{cases} \tag{2}$$

At Disease-free equilibrium $I^* = R^* = 0$, the DFE point is written as $(S^*, 0, 0, V_1^*, V_2^*, V_3^*, V_4^*)$. Solving for S^* from (2) in the first equation, we obtain

$$S^* = \frac{\Lambda + \sum_{i=1}^{4} V_i^* \epsilon_i}{\mu + \eta_1 \rho_1}$$

Then solving for $V_1^*, V_2^*, V_3^*, and \quad V_4^*$ yields the DFE point as

$$\left(\frac{\Lambda + \sum_{i=1}^{4} V_i^* \epsilon_i}{\mu + \eta_1 \rho_1}, 0, 0, \frac{\eta_1 \rho_1 S^*}{\mu + \epsilon_1 + \eta_2 \rho_2}, \frac{\eta_2 \rho_2 V_1^*}{\mu + \epsilon_2 + \eta_3 \rho_3}, \frac{\eta_3 \rho_3 V_2^*}{\mu + \epsilon_3 + \eta_4 \rho_4}, \frac{\eta_4 \rho_4 V_3^*}{\mu + \epsilon_4} \right)$$

3.4 Basic Reproductive Number ($\mathcal{R}_0$)

The reproductive number plays a crucial role in determining whether the malaria infection will die out or persist as vaccination is introduced over time in the system.

Lemma 3. *The disease-free equilibrium state is locally asymptotically stable if* $\mathcal{R}_0 < 1$ *and unstable if* $\mathcal{R}_0 > 1$.

Identify the compartments associated with infected individuals. Let $\mathbf{x} = (x_1, x_2, \ldots, x_n)^T$ be the number of infected persons in each compartment, where the first $m < n$ contains the infected individuals. We assume that x_0 is stable at disease-free equilibrium then we consider the equation $\frac{dx_i}{dt} = f_i(x) - v_i(x)$ for $i = 1, 2, 3, \ldots, m$. Using the next generation matrix approach, the f_i and v_i matrices are obtained from the infection compartment as;

$$f_1 = [\alpha S I] \quad \text{and} \quad v_1 = [(\beta + \delta + \mu) I] \tag{3}$$

$$F = \left[\frac{\partial f_1}{\partial I} \right] = [\alpha S] \quad \text{and} \quad V = \left[\frac{\partial v_1}{\partial I} \right] = [(\beta + \delta + \mu)]$$

Solving F at disease-free equilibrium, we have

$$F = \alpha \left(\frac{\Lambda + \sum_{i=1}^{4} V_i^* \epsilon_i}{\mu + \eta_1 \rho_1} \right)$$

$$FV^{-1} = \frac{\alpha(\Lambda + \sum_{i=1}^{4} V_i^* \epsilon_i)}{(\mu + \eta_1 \rho_1)(\beta + \delta + \mu)}$$

Therefore,

$$\mathcal{R}_0 = \frac{\alpha(\Lambda + \sum_{i=1}^{4} V_i^* \epsilon_i)}{(\mu + \eta_1 \rho_1)(\beta + \delta + \mu)}$$

3.5 Local Stability of Disease-free Equilibrium Point

To assess the stability of the model at its disease-free equilibrium point, we evaluate the eigenvalues of the Jacobian matrix computed at the equilibrium solution. This helps us analyze how the model population behaves near its equilibrium state over a period. Hence, we confirm the conditions that

must be fulfilled for the disease to be completely eradicated from the population and for the disease-free equilibrium state to remain stable. The Jacobian matrix of the model equations is given as ;

$$J = \begin{bmatrix} -\alpha I - \mu - \rho_1 & -\alpha S & \gamma & \epsilon_1 & \epsilon_2 & \epsilon_3 & \epsilon_4 \\ \alpha I & \alpha S - \beta - \delta - \mu & 0 & 0 & 0 & 0 & 0 \\ 0 & \beta & -\gamma - \mu & 0 & 0 & 0 & 0 \\ \rho_1 & 0 & 0 & -\mu - \epsilon_1 - \rho_2 & 0 & 0 & 0 \\ 0 & 0 & 0 & \rho_2 & -\mu - \epsilon_2 - \rho_3 & 0 & 0 \\ 0 & 0 & 0 & 0 & \rho_3 & -\mu - \epsilon_3 - \rho_4 & 0 \\ 0 & 0 & 0 & 0 & 0 & \rho_4 & -\mu - \epsilon_4 \end{bmatrix} \tag{4}$$

Theorem 4. *The system of equations (1) is considered locally asymptotically stable if all eigenvalues of the Jacobian at the disease-free equilibrium state are negative.*

Proof. Hence at the disease-free equilibrium point, the Jacobian matrix is given as

$$J(E_0) = \begin{bmatrix} -(\mu + \eta_1\rho_1) & \frac{\alpha(\Lambda + \sum_{i=1}^{4} V_i^* \epsilon_i)}{(\mu + \eta_1\rho_1)} & \gamma & \epsilon_1 & \epsilon_2 & \epsilon_3 & \epsilon_4 \\ 0 & \frac{\alpha(\Lambda + \sum_{i=1}^{4} V_i^* \epsilon_i)}{\mu + \eta_1\rho_1} - (\beta + \delta + \mu) & 0 & 0 & 0 & 0 & 0 \\ 0 & \beta & -(\gamma + \mu) & 0 & 0 & 0 & 0 \\ \eta_1\rho_1 & 0 & 0 & -(\mu + \epsilon_1 + \eta_2\rho_2) & 0 & 0 & 0 \\ 0 & 0 & 0 & \eta_2\rho_2 & -(\mu + \epsilon_2 + \eta_3\rho_3) & 0 & 0 \\ 0 & 0 & 0 & 0 & \eta_3\rho_3 & -(\mu + \epsilon_3 + \eta_4\rho_4) & 0 \\ 0 & 0 & 0 & 0 & 0 & \eta_4\rho_4 & -(\mu + \epsilon_4) \end{bmatrix}$$

The eigenvalues (λ) of the Jacobian matrix at disease-free equilibrium point are as follows

$$\lambda_1 = -(\mu + \eta_1\rho_1), \quad \lambda_2 = \left(\frac{\alpha(\Lambda + \sum_{i=1}^{4} V_i^* \epsilon_i)}{\mu + \eta_1\rho_1} \right) - (\beta + \delta + \mu), \quad \lambda_3 = -(\gamma + \mu) \tag{5}$$

$$\lambda_4 = -(\mu + \epsilon_1 + \eta_2\rho_2), \quad \lambda_5 = -(\mu + \epsilon_2 + \eta_3\rho_3), \quad \lambda_6 = -(\mu + \epsilon_3 + \eta_4\rho_4), \quad \lambda_7 = -(\mu + \epsilon_4).$$

All eigenvalues must be negative for the disease-free equilibrium to be locally asymptotically stable. For λ_2 to be negative, we have

$$\left(\frac{\alpha(\Lambda + \sum_{i=1}^{4} V_i^* \epsilon_i)}{\mu + \eta_1\rho_1} \right) - (\beta + \delta + \mu) < 0.$$

Hence, we have

$$\alpha(\Lambda + \sum_{i=1}^{4} V_i^* \epsilon_i) < (\beta + \delta + \mu)(\mu + \eta_1\rho_1). \tag{6}$$

Therefore, the disease-free equilibrium is locally asymptotically stable. □

3.6 Global Stability at Disease-free equilibrium Point

Global stability at a disease-free equilibrium point describes the behaviour of the dynamical system (1) across its entire state space. It indicates that irrespective of initial conditions, the system's trajectories converge to the disease-free equilibrium over time. The implications of global stability aid in assessing the effectiveness of interventions like vaccination programs or public health policies to eliminate malaria.

Theorem 5. *The system is globally asymptotically stable if and only if* $\mathcal{R}_0 < 1$.

Proof. The global behaviour of the disease-free equilibrium for the model is studied by constructing a Lyapunov function L at DFE. The function is defined as

$$L = I \tag{7}$$

where,

$$I = \text{the number of infected individuals.}$$

Next, we solve the derivative of the function. Thus,

$$\dot{L} = \frac{dI}{dt}$$

Now, we substitute the systems of equation (1) into $\dot{L}$. So we have

$$\dot{L} = (\alpha S - (\beta + \delta + \mu))I \tag{8}$$

Substituting S^* at disease-free, we have

$$\dot{L} = \left(\frac{\alpha(\Lambda + \sum_{i=1}^{4} V_i^* \epsilon_i)}{(\mu + \eta_1 \rho_1)} - (\beta + \delta + \mu)\right) I$$

Simplifying, we have

$$\dot{L} = (\beta + \delta + \mu)\left(\frac{\alpha(\Lambda + \sum_{i=1}^{4} V_i^* \epsilon_i)}{(\mu + \eta_1 \rho_1)(\beta + \delta + \mu)} - 1\right) I$$

Thus,

$$\dot{L} = (\beta + \delta + \mu)(\mathcal{R}_0 - 1)I(t). \tag{9}$$

□

If the derivative of the Lyapunov function is non-decreasing over time [6], thus $\dot{L} \leq 0$, then the disease-free equilibrium point is globally asymptotically stable if and only if

1. Given that $I > 0$ and $(\beta + \delta + \mu) > 0$, then $(\mathcal{R}_0 - 1) < 0$ thus $\mathcal{R}_0 < 1$.
2. If $\mathcal{R}_0 = 1$ then

$$\dot{L} = (\beta + \delta + \mu)(\mathcal{R}_0 - 1)I(t) = (\beta + \delta + \mu)(1 - 1)I(t) \implies \dot{L} = 0. \tag{10}$$

Thus, $\dot{L} \leq 0$ trivially holds if $\mathcal{R}_0 = 1$. Therefore, the system is globally asymptotically stable.

3.7 Endemic Equilibrium (EE) Point

The endemic equilibrium point is a state where the disease persists in the population indefinitely and cannot be eradicated. The endemic equilibrium point (EE) $= (S^+, I^+, R^+, V_1^+, V_2^+, V_3^+, V_4^+)$. At endemic equilibrium point, $I^+ \neq 0, R^+ \neq 0$.

Solving for S^+ in the second equation of the system of equations (1), we obtain

$$S^+ = \frac{\beta+\delta+\mu}{\alpha} \quad I^+ = \frac{R^+(\gamma+\mu)}{\beta} \quad R^+ = \frac{\beta I^+}{\gamma+\mu} \quad \text{and} \quad V_1^+ = \frac{(\beta+\delta+\mu)\eta_1\rho_1}{\alpha(\mu+\epsilon_1+\eta_2\rho_2)} \tag{11}$$

$$V_2^+ = \frac{(\beta+\delta+\mu)\eta_1\rho_1\eta_2\rho_2}{\alpha(\mu+\epsilon_1+\eta_2\rho_2)(\mu+\epsilon_2+\eta_3\rho_3)} \quad \text{and} \quad V_3^+ = \frac{(\beta+\delta+\mu)\eta_1\rho_1\eta_2\rho_2\eta_3\rho_3}{\alpha(\mu+\epsilon_1+\eta_2\rho_2)(\mu+\epsilon_2+\eta_3\rho_3)(\mu+\epsilon_3+\eta_4\rho_4)}$$

Solving for V_4^+ in the seventh equation, we obtain:

$$V_4^+ = \frac{(\beta+\delta+\mu)\eta_1\rho_1\eta_2\rho_2\eta_3\rho_3\eta_4\rho_4}{\alpha(\mu+\epsilon_1+\eta_2\rho_2)(\mu+\epsilon_2+\eta_3\rho_3)(\mu+\epsilon_3+\eta_4\rho_4)(\mu+\epsilon_4)}$$

Therefore, the solution for the endemic equilibrium point (EE)$= (S^+, I^+, R^+, V_1^+, V_2^+, V_3^+, V_4^+)$

3.8 Local Stability at Endemic Equilibrium Point

Theorem 6. *Endemic equilibrium point is locally asymptotically stable if all eigenvalues are negative.*

Proof. Consider the jacobian matrix (4) at endemic equilibrium point (EE)$= (S^+, I^+, R^+, V_1^+, V_2^+, V_3^+, V_4^+)$ such that

$$J(EE) = \begin{bmatrix} -\alpha(\frac{R^*(\gamma+\mu)}{\beta}) - \mu - \rho_1 & -\alpha(\frac{\beta+\delta+\mu}{\alpha}) & \gamma & \epsilon_1 & \epsilon_2 & \epsilon_3 & \epsilon_4 \\ \alpha(\frac{R^*(\gamma+\mu)}{\beta}) & \alpha(\frac{\beta+\delta+\mu}{\alpha}) - \beta - \delta - \mu & 0 & 0 & 0 & 0 & 0 \\ 0 & \beta & -\gamma-\mu & 0 & 0 & 0 & 0 \\ \rho_1 & 0 & 0 & -\mu-\epsilon_1-\rho_2 & 0 & 0 & 0 \\ 0 & 0 & 0 & \rho_2 & -\mu-\epsilon_2-\rho_3 & 0 & 0 \\ 0 & 0 & 0 & 0 & \rho_3 & -\mu-\epsilon_3-\rho_4 & 0 \\ 0 & 0 & 0 & 0 & 0 & \rho_4 & -\mu-\epsilon_4 \end{bmatrix}$$

Finding the eigenvalues of the jacobian matrix $|J(EE) - \lambda I = 0$ as;

$$|J(EE) - \lambda I = \begin{bmatrix} -\alpha(\frac{R^*(\gamma+\mu)}{\beta}) - \mu - \eta_1\rho_1 - \lambda & -(\beta+\delta+\mu) & \gamma & \epsilon_1 & \epsilon_2 & \epsilon_3 & \epsilon_4 \\ \alpha(\frac{R^*(\gamma+\mu)}{\beta}) & 0-\lambda & 0 & 0 & 0 & 0 & 0 \\ 0 & \beta & -\gamma-\mu-\lambda & 0 & 0 & 0 & 0 \\ \eta_1\rho_1 & 0 & 0 & -\mu-\epsilon_1-\eta_2\rho_2-\lambda & 0 & 0 & 0 \\ 0 & 0 & 0 & \eta_2\rho_2 & -\mu-\epsilon_2-\eta_3\rho_3-\lambda & 0 & 0 \\ 0 & 0 & 0 & 0 & \eta_3\rho_3 & -\mu-\epsilon_3-\eta_4\rho_4-\lambda & 0 \\ 0 & 0 & 0 & 0 & 0 & \eta_4\rho_4 & -\mu-\epsilon_4-\lambda \end{bmatrix} = 0$$

The eigenvalues of the Jacobian matrix at the endemic equilibrium point are given as:

$$\lambda_1 = -(\gamma+\mu) \quad \lambda_2 = -(\mu+\epsilon_1+\eta_2\rho_2), \quad \lambda_3 = -(\mu+\epsilon_2+\eta_3\rho_3), \tag{12}$$

$$\lambda_4 = -(\mu + \epsilon_3 + \eta_4\rho_4), \quad \lambda_5 = -(\mu + \epsilon_4)$$

$$\lambda_6 = \frac{-M - \sqrt{M^2 - 4\alpha I^+(\beta + \delta + \mu)}}{2} \quad \lambda_7 = \frac{-M + \sqrt{M^2 - 4\alpha I^+(\beta + \delta + \mu)}}{2}$$

where;

$$M = (\alpha I^+ + \mu + \eta_1\rho_1)$$

Hence, system is stable at $\lambda_1, \lambda_2, \lambda_3, \lambda_4, \lambda_5$ and λ_6. Thus, if disease prevalence deviates slightly from the endemic equilibrium, the system will naturally adjust itself back to the equilibrium over time.

To obtain this we have:

$$\lambda_7 = \frac{-M + \sqrt{M^2 - 4\alpha I^+(\beta + \delta + \mu)}}{2} < 0$$

This implies,

$$\sqrt{M^2 - 4\alpha I^+(\beta + \delta + \mu)} < M \quad \text{since} \quad M > 0 \tag{13}$$

Also considering different cases,

- Remark 1: If $M^2 - 4\alpha I^+(\beta + \delta + \mu) \geq 0$ with $M > 0$, local stability will be achieved at the endemic equilibrium point. This means the disease is likely to fade away.
- Remark 2: If $M^2 - 4\alpha I^+(\beta + \delta + \mu) < 0$, with $M < 0$ we obtain complex roots. This means the trajectories will spiral outward from equilibrium, showing instability and oscillatory behaviour. The equilibrium is unstable, so even small perturbations will cause the system to move away in a spiral pattern. Simplifying we have;

$$-4\alpha I^+(\beta + \delta + \mu) < 0. \tag{14}$$

Therefore, the endemic equilibrium point is locally asymptotically stable.

□

4 Sensivity Analysis

In epidemiology, the value of $\mathcal{R}_0$ determines the potential of the disease to spread or persist within the population. We determine the reduction in infection due to the disease by assessing how interventions—such as vaccination, public health measures, and changes in behavior—lower the reproduction number. To ascertain the influence of individual parameters on the transmission and spread of malaria, we conduct a sensitivity analysis of the model (1) with a specific emphasis on the effects of malaria vaccination using Partial Rank Correlation Coefficient (PRCC). It involves systematically varying each parameter in table 2 within a specified range and observing how parameter changes affect the model's predictions or outcomes.

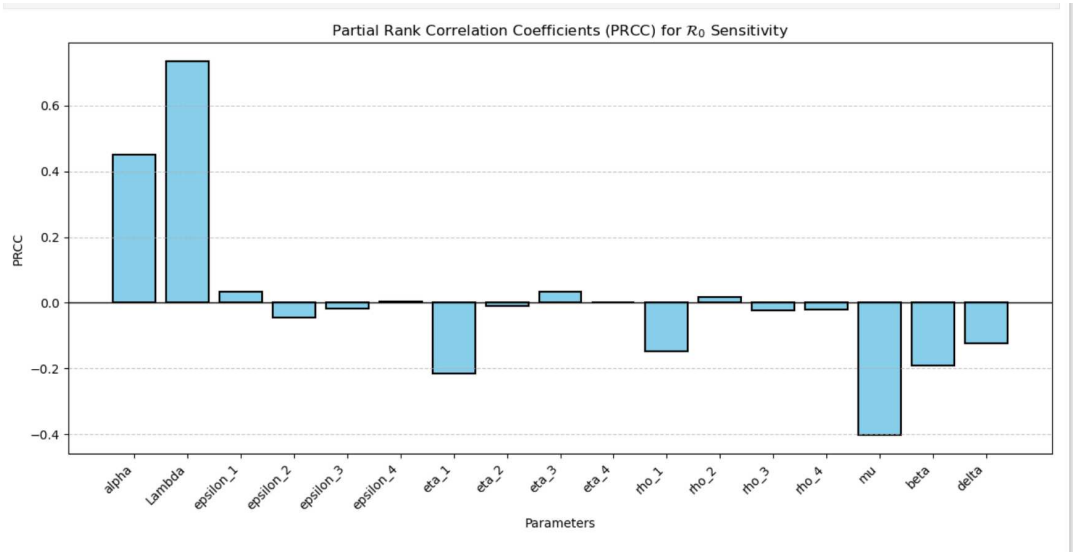

Figure 2 Partial Rank Correlation Coefficients (PRCC) for $\mathcal{R}_0$ Sensitivity

The positive sensitivity index indicates that an increase (or decrease) in the value of each parameter leads to a corresponding increase (or decrease) in the spread of the disease ($\mathcal{R}_0$). Conversely, the negative sensitivity index indicates that an increase (or decrease) in the value of each parameter leads to a corresponding decrease (or increase) in the disease spread ($\mathcal{R}_0$).

5 Numerical Simulation

To graphically examine the progress of the RTS,S/AS01 vaccination in eradicating malaria in Ghana over time, we conduct numerical simulations on the model's system of equations(1). These simulations focus specifically on assessing the impact of the malaria vaccination in reducing and eradicating the disease. The simulations are implemented in Python, utilizing parameters presented in Table (2). Parameters used in the simulations are obtained from research papers, with some being reasonable estimates. We use Ghana's infant population data (2023) [23] as stated in the literature review to estimate our initial conditions: $S(0) = 2,759,223; I(0) = 900,000; R(0) = 300,000$. We use the following information on the RTS,S/AS01 vaccination stages are as follows: $V_1(0) = 96,245; V_2(0) = 88,348; V_3(0) = 64,559; V_4(0) = 41,625$.

Parameter	Values	Reference
Λ	0.0277	[10]
α	0.086	[16]
β	0.067841	[12]
γ	0.01	Estimated
δ	0.0308	[10]
μ	0.0154	[12]
ρ_1	0.03	Estimated
ρ_2	0.02	Estimated
ρ_3	0.015	Estimated
ρ_4	0.005	Estimated
η_1	0.3	Estimated
η_2	0.4	Estimated
η_3	0.5	Estimated
η_4	0.8	Estimated
ϵ_1	0.01	Estimated
ϵ_2	0.005	Estimated
ϵ_3	0.0003	Estimated
ϵ_4	0.0001	Estimated

Table 2 Numerical Values and References for Parameters

5.1 Simulations of Malaria Vaccination Model

In this section, we simulate the model to graphically view and understand the population dynamics with vaccination implemented to eliminate the malaria disease, reduce malaria death-induced rates and increase recoveries. Figure (3) graphically examines the vaccine's efficacy over 300 days in the population.

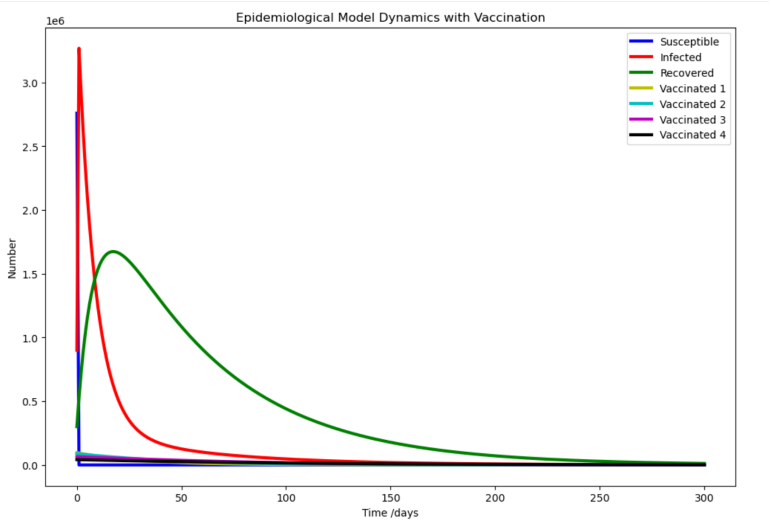

Figure 3 Dynamics of the post-malaria vaccination population over 300 days

Figure (3) describes the dynamics of the different population groups (Susceptible, Infected, Recovered, and Vaccinated at four levels) over time. In this population dynamics, the susceptible infants decrease over time due to infants receiving vaccinations as well as some becoming infected. Also, the number of infected infants initially shows a rise, reflecting the spread of the infection in the population. Over time, the infected population peaks and then declines. This shows the effectiveness of the vaccination minimises the number of new infections and increases the number of recoveries. Recovered infants increase and then decrease while the vaccinated populations at various levels show gradual changes reflecting the progression through vaccination stages.

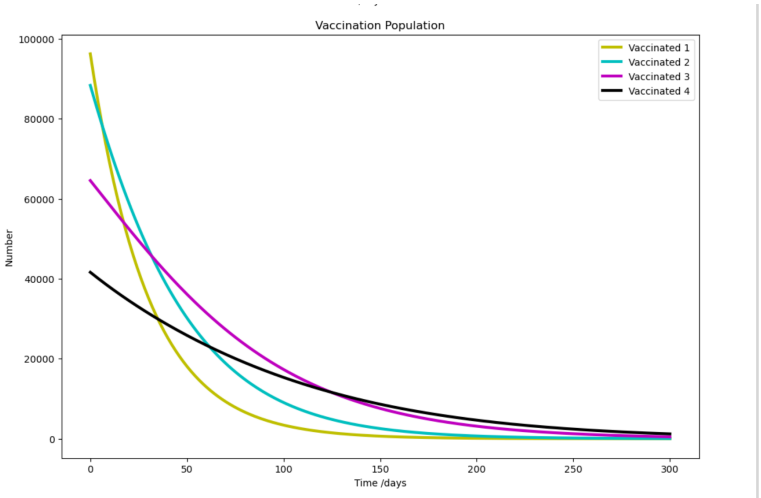

Figure 4 Dynamics of the post-malaria vaccination population over 300 days

Figure (4) describes the number of individuals in each stage of vaccination over time. The curves start with high numbers at the initial vaccination stage and decrease progressively through the subsequent stages. This indicates that as the vaccination campaign progresses, fewer individuals remain in

each stage with the highest initial numbers receiving the first dose and a gradual decline as they move through to the final dose. As the efficacy of the vaccine wanes, the vaccinated population decreases transitioning back into the susceptible population. This is illustrated by the gradual decline in the vaccinated population as efficacy reduces. A complete vaccination dose immunizes the infant for a long period.

6 Data Description

This chapter focuses on utilizing deep data-driven models to simulate the impact of malaria vaccination. Due to the unavailability of real-world data, we use generated data to mirror real-life scenarios. The neural network operates within Python and the popular machine learning library, "TensorFlow" and "Keras" are used to generate and train data. This generated data will be used to test various Neural Network (NN) models. The process begins with the generation of datasets that replicate the dynamics of malaria transmission and vaccination. Using the Disease Informed Neural Network (DINN), we let DINN learn and estimate the epidemiological parameters from the generated data to confirm the numerical values in table 2. The parameters that have been learned will be sent into an ODE numerical solver to generate graphs that illustrate how various vaccination approaches affect the spread and management of malaria. The resulting graphs will help determine the best vaccination plans and show how changing the parameters can impact the spread of the disease.

7 Algorithm for Malaria Vaccination Model Using Deep Data-Driven Methods

The algorithm states the approach for simulating the impact of malaria vaccination using deep data-driven models, particularly in scenarios where real-life data is unavailable. The process combines neural network learning with epidemiological modelling to forecast and analyze the effects of different vaccination strategies on malaria.

1. Perform data pre-processing by normalizing the generated data and splitting the data into training, validating and testing sets.

2. Using our selected Neural Network models (ResNet, LSTM, BiLSTM, and GRU, ResNet-LSTM, ResNet-BiLSTM, ResNet-GRU), we configure our layers (input, hidden and output layers).

3. We used TensorFlow and Keras to train the model, validate and save the learned parameters. We specified Mean Squared Error (MSE) as the loss function and applied the Adam optimizer along with k-fold validation for performance assessment.

4. The learned parameters are extracted from the trained neural network and are used in our epidemiological model of ordinary differential equations (ODEs) (1)

5. Using the ODE solver with our learned parameters, we simulate malaria dynamics under different and constant vaccination strategies with corresponding different and constant efficacy rates.

6. We visualize our results using plots and bar graphs to depict each model's performance in terms of reliability and accuracy in forecasting and predicting daily infected cases as well as illustrating the impact of various vaccination and efficacy strategies.

8 Data-driven Simulations

The Disease Informed Neural Network (DINN) is used to learn the values of each parameter. This is performed using *"tilda"*. Tilda sets the values within a specific range. The values of learned parameters are either the same or close to the actual values used in table 2. Table 3 displays the actual values and the learned parameter values.

Parameter	Actual Values	DINN Learned Values
Λ	0.0277	0.0277
α	0.0860	0.0858
β	0.067841	0.0677
γ	0.0100	0.0100
δ	0.0308	0.0308
μ	0.0154	0.0154
ρ_1	0.0300	0.0300
ρ_2	0.0200	0.0200
ρ_3	0.0150	0.0150
ρ_4	0.0050	0.0050
η_1	0.3000	0.2913
η_2	0.4000	0.3799
η_3	0.5000	0.4621
η_4	0.8000	0.6644
ϵ_1	0.0100	0.0100
ϵ_2	0.0050	0.0050
ϵ_3	0.0003	0.0003
ϵ_4	0.0001	0.0001

Table 3 Actual Values vs DINN Learned Values

The DINN algorithm is used to learn different values of α and β for random vaccination dose rates. We assume these rates are constant over a few months of vaccination. The goal is to study how effective full vaccination dosage and variations in vaccination rates are efficient in reducing infections to zero quickly. These values with the learned parameters are used to run numerical simulations for modelling (1) [20]. Table 4 shows the impact of constant vaccination rate at 0.7% efficacy with different α, $\beta \in [0.1, 0.5]$ to produce different $\mathcal{R}_0$ for the entire period.

Vaccination rate (ρ_i)	α	β	$\mathcal{R}_0$
0%	0.38	0.15	4.8977
1%	0.30	0.14	1.96219
2%	0.40	0.21	1.8586
3%	0.40	0.21	1.4540
4%	0.18	0.13	0.76821
5%	0.45	0.40	0.56632
8%	0.45	0.40	0.341507
10%	0.15	0.10	0.28035

Table 4 Impact of Vaccination at efficacy = 0.7%

The graph in Figure (5) (6) compares the actual simulations in Figure 3 and Figure 4 to the predicted simulations generated after the neural network has learned the parameters. Figure (7) presents the model with a constant vaccination rate ($\rho_i = 0.7\%$) and initial vaccine efficacy at each level. The result displays an infected population percentage of 0.5987%.

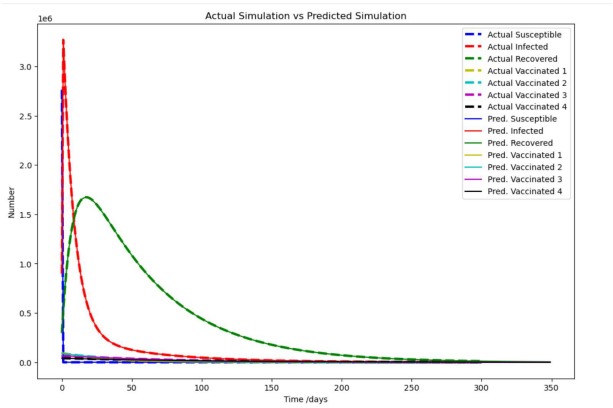

Figure 5 Actual model vs Predicted model

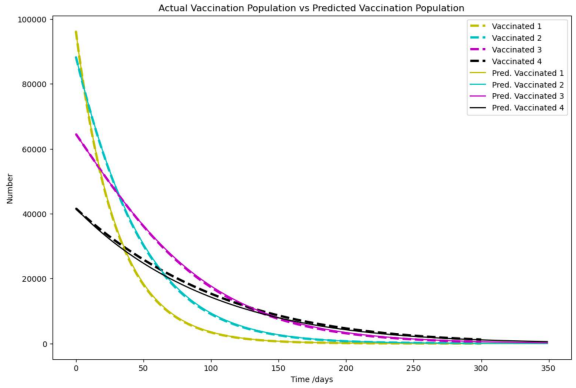

Figure 6 Actual Vaccination population vs Predicted Vaccination population

Figure 8 shows the population dynamics of the generated malaria vaccination data without vaccination. The absence of vaccination increases malaria infection to 0.8292% which corresponds to approximately 3,524,291 recorded infection cases.

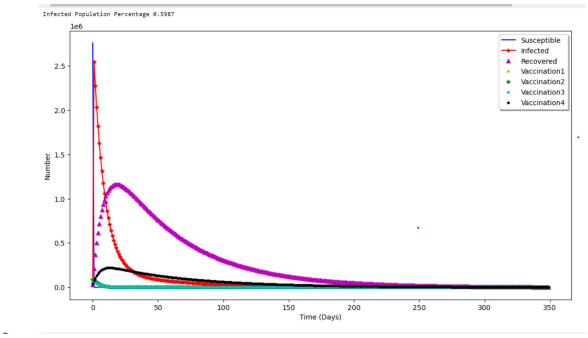

Figure 7 Population Dynamics with constant vaccination rate, $\rho_i = 0.7\%$

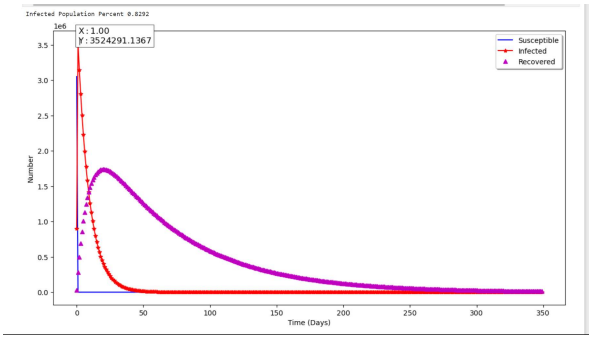

Figure 8 Model without vaccination.

The table 5 shows the impact of constant vaccination rate at 0.94% efficacy with different α, $\beta \in [0.1, 0.5]$ to produce different R_0 for the entire period. At different vaccination rates with different α and β, it is shown that the spread of malaria disease will die out when vaccination rate, $\rho_i = 90\%$ with vaccine efficacy, $\eta_i = 0.94\%$ gives the Reproductive number, $\mathcal{R}_0 = 0.00068077$.

Vaccination rate (ρ_i)	α	β	$\mathcal{R}_0$
0%	0.38	0.15	4.8977
1%	0.44	0.22	2.3581
5%	0.45	0.23	0.84778
10%	0.42	0.22	0.570958
30%	0.43	0.24	0.140668
50%	0.27	0.16	0.097347
70%	0.17	0.13	0.042793
90%	0.03	1.55	0.00068077

Table 5 Impact of Vaccination at efficacy = 0.94%

The population dynamics when the vaccine efficacy rate increases at each *ith* level ($\eta_1 = 0.5$, $\eta_2 = 0.7$, $\eta_3 = 0.85$, $\eta_4 = 0.94$) while maintaining a constant vaccination rate of $\rho_i = 0.9\%$ is depicted in Figure 9. As the vaccination population increases over time, the percentage of the infected population decreases to 27.98%. Conversely, Figure 10 illustrates the impact of a decreasing vaccination rate at each *ith* level ($\rho_1 = 0.94\%, \rho_2 = 0.85\%, \rho_3 = 0.75\%, \rho_4 = 0.65\%$) for different vaccine efficacies ($\eta_1 = 0.5$, $\eta_2 = 0.7$, $\eta_3 = 0.85$, $\eta_4 = 0.94$). As the vaccination rate reduces at each stage, the percentage of the infected population increases slightly from 27.98% to 28.34%.

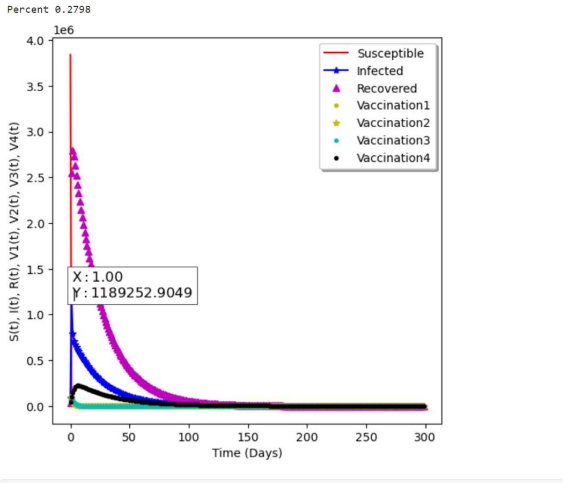

Figure 9 Population Dynamics with vaccination rate $\rho_i = 0.9\%$

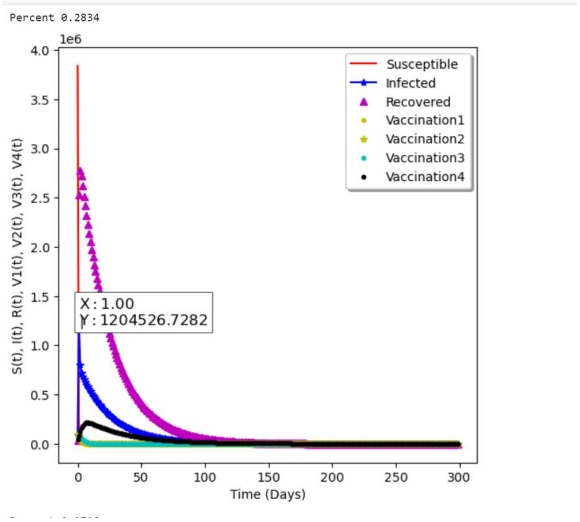

Figure 10 Population dynamics with different vaccination and vaccine efficacy rates

Table 6 presents the parameter settings for different machine-learning approaches used in the neural network. Every approach has distinct settings for several parameters that are crucial for the model training.

Table 6 Parameter settings.

Approach	Parameter	Value
LSTM/BiLSTM/GRU	Learning rate	0.01
	Training Epochs	1500
	Batch Size	32
	Layers	02
	Features	01
	Neurons	16
ResNet	Learning rate	0.001
	Training Epochs	4000
	Batch Size	10
	Layers	04
	Features	01
	Neurons	50
Cross Validation	Learning rate	0.01
	Training Epochs	2000
	Batch Size	100
	Layers	01
	Features	01
	Neurons	16

The figure(11) shows the data-driven simulation for learning the infected cases using ResNet compared with the daily infected cases. To conduct the comparative analysis, the results obtained from the ResNet model are compared with the daily count of infected cases. The output cases of GRU, LSTM and BiLSTM are plotted against the generated infected cases as shown in Figure 12, Figure 13 and Figure 14 accordingly.

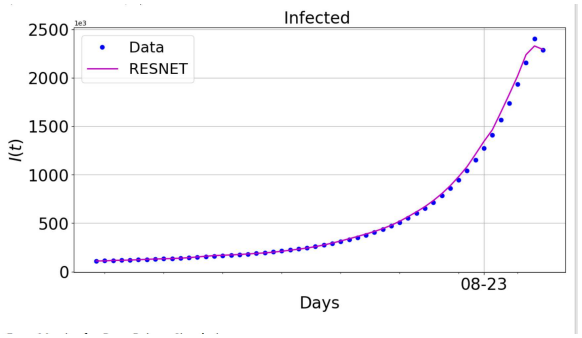

Figure 11 Simulation of malaria vaccination data and ResNet outcomes

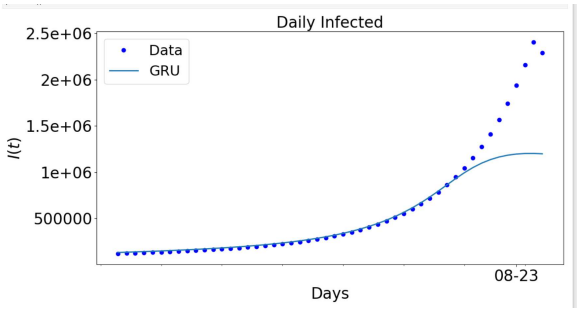

Figure 12 Simulation of malaria vaccination data and GRU outcomes

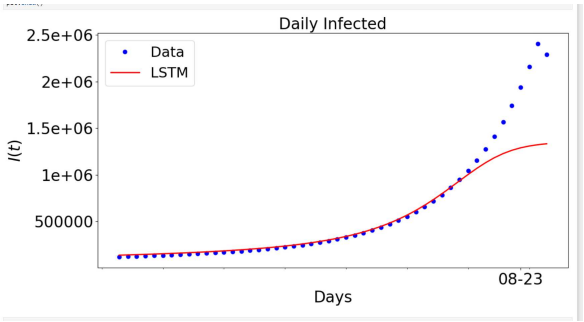

Figure 13 Simulation of malaria vaccination data and LSTM outcomes

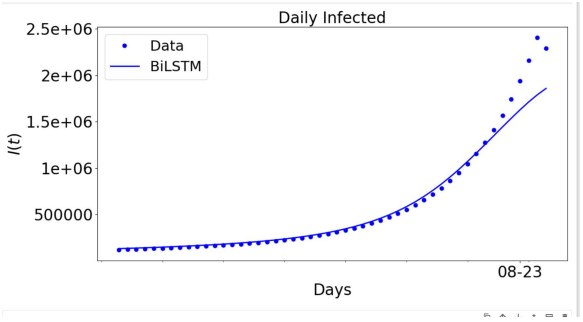

Figure 14 Simulation of malaria vaccination data and BiLSTM outcomes

The output from LSTM, BiLSTM, and GRU are plotted together along with the daily infected cases. Figure 15 evaluates how well each model (GRU, LSTM, BiLSTM) predicts the real data trends over time. BiLSTM model provides closer predictions along the lines of the actual daily infected cases compared to the other two models (GRU and LSTM).

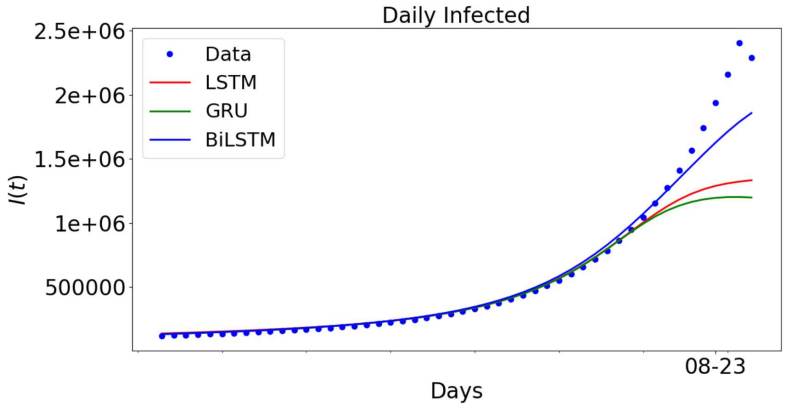

Figure 15 Data-driven simulations for BiLSTM, GRU and LSTM

The hybrid approach involving ResNet is combined with LSTM, BiLSTM, and GRU models (ResNet-BiLSTM, ResNet-LSTM, and ResNet-GRU). The ResNet model's output serves as the input data for these sequential models. Table 6 outlines the specific parameter settings for each hybrid approach. Figure 16 shows the hybrid cases plotted along the daily infected cases. The ResNet model's output (data) is used to train the other three models (LSTM, GRU, BiLSTM). Based on the generated data and the different hybrid approaches, the best model is given as the ResNet-GRU as predictions is much closer to the daily cases.

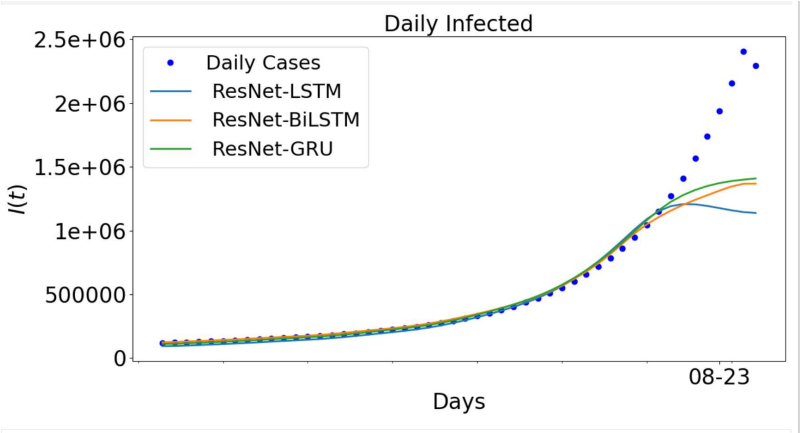

Figure 16 Data-driven simulations for ResNet-BiLSTM, RestNet-GRU and ResNet-LSTM

9 Error Metrics from Data-Driven Simulations

Error metrics from data simulations are quantitative measures used to determine the performance of the data-driven simulations by comparing the model's predictions to the actual generated observed data. They are used in evaluating the accuracy and reliability of the predicted models. The Error metrics from the generated malaria vaccination data and ResNet are shown in table 7. The table shows that BiLSTM has the smallest **RMSE** and **MAPE** (relative error) with 421495.166 and 0.239608 respectively. In addition, the model with the greatest **EV** (error value) is BiLSTM. This implies that

the BiLSTM model gives the best error values for the generated malaria vaccination data.

Approach	RMSE	MAPE	EV
LSTM	644321.756	0.366274	0.30217
BiLSTM	421495.166	0.239608	0.671984
GRU	603323.937	0.342972	0.403436
ResNet-LSTM	677850.125	0.365410	0.2953
ResNet-BiLSTM	634516.25	0.342050	0.40291
ResNet-GRU	615500.875	0.331799	0.404994

Table 7 Error Metrics from Data-Driven Simulations

Figure 17 shows the RMSE and MAPE values for each model approach. The metrics of both graphs show that the model approach with the least error value is BiLSTM.

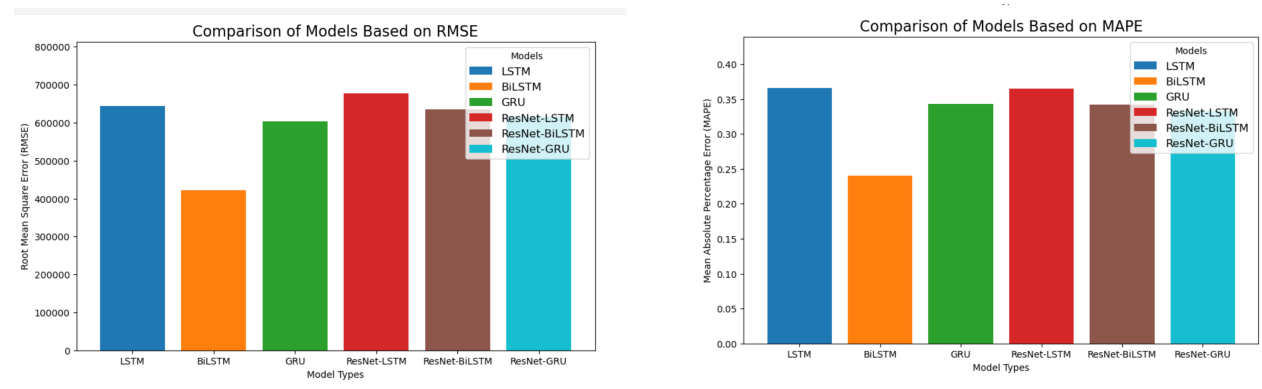

Figure 17 The graph of RMSE and MAPE values for model each approach.

Figure 18 gives the error values (EV) of each model approach. The model with the biggest EV is BiLSTM. Three key error metrics are used to evaluate how well each algorithm captures the underlying dynamics: RMSE, MAPE, and EV. RMSE indicates accuracy; lower values are better. EV near 1 shows consistent predictive performance of the neural network.

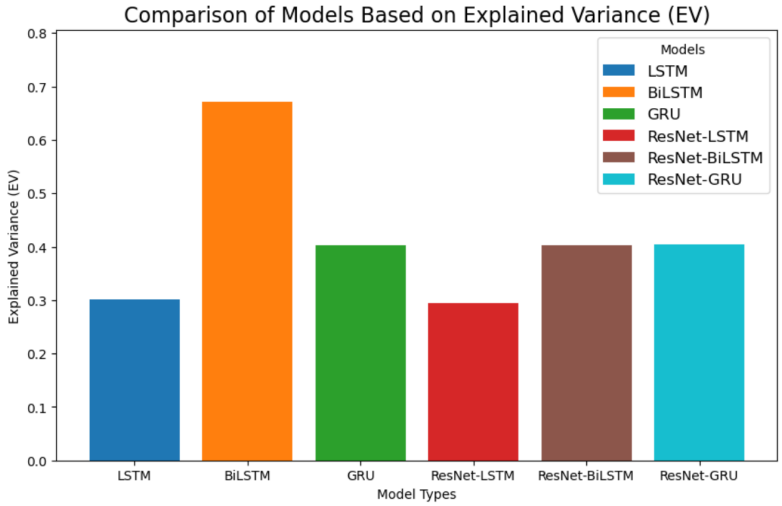

Figure 18 The graph of EV values for each approach

10 k-Fold Cross Validation

The average RSME for all k values is plotted for each model using a bar graph. This technique of dividing the data into k subsets (folds) helps to evaluate the performance of all models to generate a reliable estimate of their accuracy and capacity for generalization when the results are averaged for the generated malaria vaccination data. When k=4, the highest value is BiLSTM followed slightly less by GRU then LSTM with the lowest value. When k=5, the highest value is GRU followed by BiLSTM then LSTM with lower value variations. When k=6, the lowest value is LSTM followed by BiLSTM then GRU. When k=7, the highest value is BiLSTM followed by GRU then LSTM.

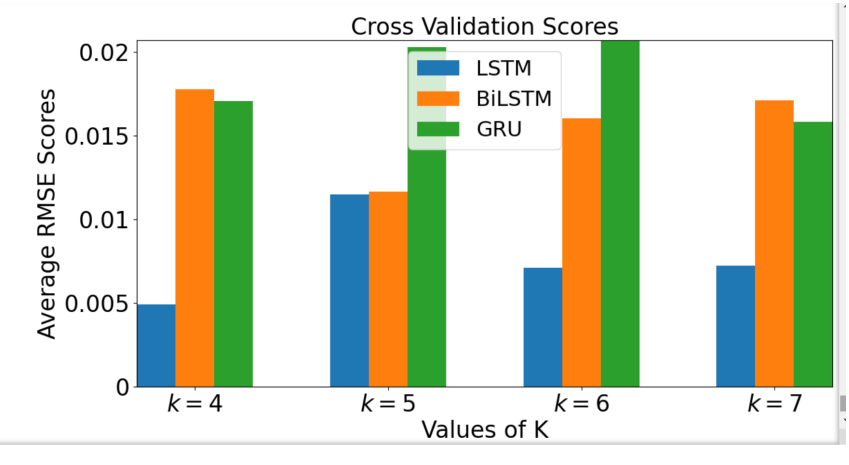

Figure 19 Cross Validation Scores using mean scores for each value of k for the generated Malaria Vaccination data

The average RSME for all k values is plotted for each model using a bar graph for the ResNet data. Figure 20 displays the cross-validation scores for the generated data. When k=4, 5 and 6, the model

with the least value is ResNet-LSTM followed by ResNet-BiLSTM then ResNet-GRU. When k=7, the highest value is ResNet-GRU followed by ResNet-BiLSTM then ResNet-LSTM but the difference in values between ResNet-GRU and ResNet-BiLSTM is not much compared to the same models in other k values.

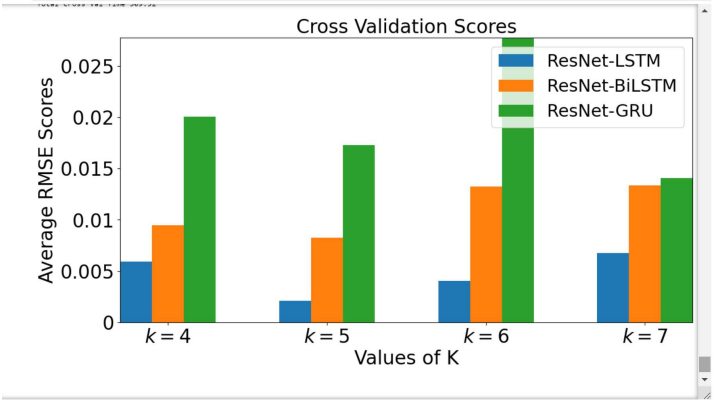

Figure 20 Cross Validation Scores using mean scores for each value of k for ResNet data

11 Conclusion

The study presented and analyzed mathematical models to evaluate the impacts of malaria vaccination programs specifically focusing on the RTS,S/AS01 malaria vaccine to eliminate the disease for infants under 5 in Sub-Sahara Africa narrowing to Ghana. The study provides valuable insights into how the vaccine components can help limit the spread of malaria in both endemic and non-endemic situations. The formulated model describes the dynamics of susceptible, infected, and different vaccinated populations. The model was tested for boundedness (feasibility) and accuracy (positivity) in representing real-life scenarios showing their capability to simulate the effects of malaria vaccination in a Ghanaian community setting. Our qualitative analysis reveals that the implemented vaccination program can stabilize and potentially eradicate malaria within a population. This outcome is observed in both Disease-free and Endemic equilibrium states. The vaccination program's success depends on its ability to lessen the basic reproduction number $\mathcal{R}_0$ below 1 indicating a controlled and eventually declining infection rate. The models highlight critical parameters influencing malaria spread (sensitivity index) using the PRCC chart. Numerical simulations were performed to graphically view and analyze the population dynamics for over 300 days. Initial values were obtained from past literature and some reasonable estimates as well as real vaccination data from MVIP monthly data 2023 bulletin-Ghana. We found out that lower vaccination rates at each level increase infections hence reducing the recovery population. These insights are invaluable for policymakers offering data-driven guidance on optimizing vaccination strategies to control malaria transmission effectively.

We integrated machine learning tools to deepen our understanding of our population dynamics under varying vaccination rates applying deep-data-driven models to simulate and predict epidemiological parameters. Data was generated to simulate real-world vaccination scenarios allowing us to explore different vaccination strategies and their impacts on the disease dynamics. Using advanced neural networks such as ResNet, LSTM, GRU, and BiLSTM, we trained our models to predict disease spread accurately along the generated data to suggest the best model for forecasting. ResNet emerged as the most effective model and for our Recurrent Neural Network types, the best model was BiLSTM,

LSTM, and GRU. We also tested hybrid models that combine recurrent and residual neural networks to forecast future infection rates. The hybrid model, ResNet-GRU was particularly successful achieving the highest Explained Variance (EV) and the lowest Root Mean Squared Error (RMSE) and Mean Absolute Percentage Error (MAPE).

Our findings indicate that maintaining a high and consistent vaccination rate across all stages of malaria is crucial. Increased vaccine efficacy and widespread coverage can significantly reduce the number of infected cases leading to potential eradication. The models developed in this study are suitable for both endemic and non-endemic areas offering a flexible tool for predicting and managing malaria outbreaks.

Acknowledgement

Esi thanks the African Institute of Mathematics, Mbour, Senegal for one year funding towards graduate studies.

References

[1] Abaka-Quansah, E. (2024). Deep data-driven neural network for malaria vaccination model. Master's thesis, African Institute of Mathematical Science (AIMS), Senegal.

[2] Adadi, A. (2021). A survey on data-efficient algorithms in big data era. *Journal of Big Data*, 8(1):24.

[3] Alamo, T., Reina, D. G., Gata, P. M., Preciado, V. M., and Giordano, G. (2021). Data-driven methods for present and future pandemics: Monitoring, modelling and managing. *Annual Reviews in Control*, 52:448–464.

[4] Brunton, S. L., Proctor, J. L., and Kutz, J. N. (2016). Discovering governing equations from data by sparse identification of nonlinear dynamical systems. *Proceedings of the national academy of sciences*, 113(15):3932–3937.

[5] Hill, A. V. (2011). Vaccines against malaria. *Philosophical Transactions of the Royal Society B: Biological Sciences*, 366(1579):2806–2814.

[6] Hinze, M., Schmidt, A., and Leine, R. I. (2020). The direct method of lyapunov for nonlinear dynamical systems with fractional damping. *Nonlinear Dynamics*, 102(4):2017–2037.

[7] Ijeh, S., Okolo, C. A., Arowoogun, J. O., Adeniyi, A. O., and Omotayo, O. (2024). Predictive modeling for disease outbreaks: a review of data sources and accuracy. *International Medical Science Research Journal*, 4(4):406–419.

[8] Kang, J. and Raimbault, J. (2023). Exploring and optimising infectious disease policies with a stylised agent-based model. In *French Regional Conference on Complex Systems*, pages 179–196.

[9] Kuhl, E. (2021). *Computational epidemiology*. Springer.

[10] Macrotrends (2023). Ghana birth rate 1950-2023. Accessed: 2024-05-29.

[11] Moorthy, V. S., Good, M. F., and Hill, A. V. (2004). Malaria vaccine developments. *The lancet*, 363(9403):150–156.

[12] Nana-Kyere, S., Seidu, B., and Nantomah, K. (2024). Dynamical study of malaria epidemic: Stability and cost-effectiveness analysis in the context of ghana. *Results in Control and Optimization*, page 100430.

[13] Pang, G., Lu, L., and Karniadakis, G. E. (2019). fpinns: Fractional physics-informed neural networks. *SIAM Journal on Scientific Computing*, 41(4):A2603–A2626.

[14] Raissi, M., Perdikaris, P., and Karniadakis, G. E. (2019). Physics-informed neural networks: A deep learning framework for solving forward and inverse problems involving nonlinear partial differential equations. *Journal of Computational physics*, 378:686–707.

[15] Sarker, I. H. (2021). Data science and analytics: an overview from data-driven smart computing, decision-making and applications perspective. *SN Computer Science*, 2(5):377.

[16] Severe Malaria Observatory (2023). Ghana malaria statistics.

[17] Shaier, S., Raissi, M., and Seshaiyer, P. (2021). Data-driven approaches for predicting spread of infectious diseases through dinns: Disease informed neural networks. *arXiv preprint arXiv:2110.05445*.

[18] Solomatine, D., See, L. M., and Abrahart, R. (2008). Data-driven modelling: concepts, approaches and experiences. *Practical hydroinformatics: Computational intelligence and technological developments in water applications*, pages 17–30.

[19] Strielkowski, W., Vlasov, A., Selivanov, K., Muraviev, K., and Shakhnov, V. (2023). Prospects and challenges of the machine learning and data-driven methods for the predictive analysis of power systems: A review. *Energies*, 16(10):4025.

[20] Torku, T. K., Khaliq, A. Q. M., and Furati, K. M. (2021). Deep-data-driven neural networks for covid-19 vaccine efficacy. *Epidemiologia*, 2:564–586.

[21] Venkatesan, P. (2024). Routine malaria vaccinations start in africa. *The Lancet Microbe*, 5(6):e519.

[22] World Health Organization (2020). *World Malaria Report 2020: 20 Years of Global Progress and Challenges*. World Health Organization, Geneva, Switzerland. Accessed: 2024-06-15.

[23] Worldometer (2023). Ghana population (2023). Accessed: 2024-06-11.

[24] Yang, Y. and Perdikaris, P. (2019). Adversarial uncertainty quantification in physics-informed neural networks. *Journal of Computational Physics*, 394:136–152.

[25] Zhu, Y., Zabaras, N., Koutsourelakis, P.-S., and Perdikaris, P. (2019). Physics-constrained deep learning for high-dimensional surrogate modeling and uncertainty quantification without labeled data. *Journal of Computational Physics*, 394:56–81.